fire

MDPI

Article

Transformation of NO in Combustion Gases by DC Corona

Oleksandr Molchanov [1,*], Kamil Krpec [1], Jiří Horák [1], Lenka Kuboňová [1], František Hopan [1], Jiří Ryšavý [1] and Marcelina Bury [2]

[1] Energy Research Centre, Centre for Energy and Environmental Technologies, VSB—Technical University of Ostrava, 17. listopadu 2172/15, 708 00 Ostrava, Czech Republic; kamil.krpec@vsb.cz (K.K.); jiri.horak2@vsb.cz (J.H.); lenka.kubonova@vsb.cz (L.K.); frantisek.hopan@vsb.cz (F.H.); jiri.rysavy@vsb.cz (J.R.)

[2] Department of Fuels Technology, Faculty of Energy and Fuels, AGH University of Krakow, al. A. Mickiewicza 30, 30-059 Krakow, Poland

* Correspondence: oleksandr.molchanov@vsb.cz; Tel.: +420-773286102

Abstract: This study investigates the performance of DC corona discharge electrostatic precipitators (ESPs) for NO conversion to increase DeNO$_x$ technologies' efficiency for small-scale biomass combustion systems. Experiments were conducted using a 5 kW automatic wood pellet domestic heat source with combustion gas treated in a specially designed ESP operated in both positive and negative corona modes, resulting in a reduction in NO concentrations from 130 mg/m^3 to 27/29 mg/m^3 for positive/negative polarities (at 0 °C and 101.3 kPa). NO conversion efficiency was evaluated across a range of specific input energies (SIEs) from 0 to 50 J/L. The results demonstrate that DC corona ESPs can achieve up to 78% NO reduction, with positive corona demonstrating a greater energy efficiency, requiring a lower SIE (35 J/L) compared to the negative corona mode (48 J/L). A detailed analysis of reaction pathways revealed distinct conversion mechanisms between the two modes. In positive corona, dispersed active species distribution led to more uniform NO conversion, while negative corona exhibited concentrated reaction zones with about 20% higher ozone production. The reactions involving O and OH radicals were more important in positive corona, whereas ozone-mediated oxidation dominated in negative corona. The research results demonstrate that ESP technology with DC corona offers a promising, energy-efficient solution for NO$_x$ control in small-scale combustion systems.

Keywords: electrostatic precipitator; small-scale combustion; pollution control; NO$_x$; PM

check for updates

Academic Editor: Jiaqiang E

Received: 27 November 2024
Revised: 6 January 2025
Accepted: 7 January 2025
Published: 8 January 2025

Citation: Molchanov, O.; Krpec, K.; Horák, J.; Kuboňová, L.; Hopan, F.; Ryšavý, J.; Bury, M. Transformation of NO in Combustion Gases by DC Corona. *Fire* **2025**, *8*, 21. https://doi.org/10.3390/fire8010021

Copyright: © 2025 by the authors. Licensee MDPI, Basel, Switzerland. This article is an open access article distributed under the terms and conditions of the Creative Commons Attribution (CC BY) license (https://creativecommons.org/licenses/by/4.0/).

1. Introduction

Despite advances in renewable energy, combustion dominates in the fields of power generation and heating. Biomass combustion, with particular significance in residential sectors, provided about 43% of the European Union's heat energy in 2019 and is expected to be important for the next 50 years [1]. However, the widespread use of solid fuel heating systems, particularly in residential areas, presents significant environmental and health challenges that warrant urgent attention.

Small-scale combustion units, such as domestic heating appliances, collectively contribute substantially to air pollution in many regions, especially during heating seasons. These installations, whilst providing essential heating services, often operate with lower combustion efficiency and fewer emission controls compared to their industrial counterparts. The situation is particularly concerning in densely populated areas where the cumulative effect of numerous small emission sources can significantly impact local air quality and public health.

Combustion produces hazardous pollution that profoundly impacts human health and the surrounding environment, with nitrogen oxides (NO_x) being one of the most significant contributors, causing smog, acid rain, and other environmental concerns. In the context of residential heating, NO_x emissions are particularly problematic due to the typically lower installation heights of chimneys and the proximity to populated areas.

NO makes up the vast majority, over 90%, of typical NO_x in combustion gases from mobile and landline sources. The low chemical reactivity of NO complicates the $DeNO_x$ through chemical solutions, requiring a significant amount of reagents to achieve the required efficiency [2], whereas catalysis-based technologies necessitate higher treatment temperatures [3].

Recent advancements in catalyst development have yielded promising results for NO_x reduction at lower temperatures. Notably, novel Cu-Ce bimetallic catalysts have demonstrated over 90% NO conversion within the temperature range of 180–360 °C [4], Similarly, the V_2O_5-MoO_3/TiO_2 catalyst has achieved over 90% NO conversion across a broader temperature range of 150–400 °C [5]. Also, the low-temperature NH_3-SCR catalyst technology, applied in non-electric industries, demonstrated about 90% NO conversion at 125 °C [6].

While considerable progress has been made in controlling emissions from large industrial installations, the development of effective, economically viable emission control technologies for small-scale applications remains a significant challenge. Efforts have been made to improve the combustion process, including the development of exhaust gas recirculation systems [7]; however, the effectiveness of NO_x emission reduction was not always sufficient, primarily due to the significant influence of the type of wood used.

One potential way to efficiently solve the low NO activity is the conversion of NO to more soluble NO_2 via the treatment of combustion gases with nonthermal plasma (NTP) [8], forming in electrical discharges [9]. Detailed information on TNP can be found elsewhere [10].

Extensive research on the NO transformation in NTP generated in dielectric barrier discharge (DBD) [8] and impulse corona discharge (ICD) [11] has been conducted. The DBD, represented by an assembly of filamentary micro-discharges, and ICD with an impulse duration of 10–100 ns have demonstrated efficient NO conversion; however, they can produce undesirable byproducts [12], necessitating further gas cleaning. As a result, commercial implementation of these technologies remains scarce, and their application to industrial exhaust gas cleaning is still uncertain.

Another type of discharge, the DC corona, commonly employed in electrostatic precipitators (ESPs), holds promising potential for the efficient treatment of NO in emissions and solves the issue of formatted byproducts. In contrast to DBD/ICD, the highly nonuniform electric field is a necessary condition for a DC corona to be generated, forcing the NTP to be highly inhomogeneous and restricted in a thin volume limited by the surface of the discharge electrode and an imaginary outer boundary, where the ionisation and the electron attachment reach equilibrium. The transformation of NO was considered to result from reactions with the reactive components generated in NTP by dissociation, namely ground-state oxygen atoms O, OH radicals and O_3. NO was converted through (i) the NO oxidation to NO_2 by oxygen atoms O and ozone, or (ii) NO removal by OH radicals with the formation of nitric acid vapour.

The set of reactions for NO conversion used in this study, along with the corresponding reaction rates, is presented in Table 1. This set represents the main chemical pathways for O_2 and H_2O dissociation, formation of active species (O, OH, O_3) and NO oxidation and reduction processes.

Table 1. The chemical reactions set.

No	Reaction	Reaction Constant	Reference
R1	$e + O_2 \xrightarrow{k_1} O + O + e$	$k_1 = 10^{(-7.9-13.4/(E_{(r)}/N))}$	[13]
R2	$e + H_2O \xrightarrow{k_3} OH + H + e$	$k_2 = 10^{(-9.9-31/(E_{(r)}/N))}$	[14]
R3	$O + O_2 + M \xrightarrow{k_8} O_3 + M$	$k_3 = 6.29 \times 10^{-34}(T/300)^{-2} \times [N_2]$	[15]
R4	$O_2 + O_3 \xrightarrow{k_{10}} O + 2O_2$	$k_4 = 7.3 \times 10^{-16} \times e^{(-11500/T)}$	[15]
R5	$NO + OH + M \xrightarrow{k_{11}} HNO_2 + M$	$k_{11} = 6.5 \times 10^{-31}(T/300)^{-2.4} \times [N_2]$	[15]
R6	$NO + O + M \xrightarrow{k_{13}} NO_2 + M$	$k_{13} = 1 \times 10^{-31}(T/300)^{-1.6} \times [N_2]$	[15]
R7	$NO + O_3 \xrightarrow{k_{14}} NO_2 + O_2$	$k_{14} = 1.4 \times 10^{-12}e^{-1310/T}$	[15]
R8	$NO_2 + O \xrightarrow{k_{22}} NO + O_2$	$k_{22} = 1.7 \times 10^{-11}e^{-300/T}$	[15]
R9	$HNO_2 + OH \xrightarrow{k_{27}} NO_2 + H_2O$	$k_{27} = 1.8 \times 10^{-11}e^{-390/T}$	[16]
R10	$NO_2 + O_3 \xrightarrow{k_{23}} NO + 2O_2$	$k_{23} = 1.0 \times 10^{-18}$	[16]

For usual combustion gases, the typical energy levels available in DC corona discharges are sufficient to cause significant dissociation of H_2O, with an energy threshold of 5.7 eV [17], and dissociation of O_2, which dissociates to the ground state of the oxygen atom O with dissociative energies of 6.4 eV [18], reasonably suggested to be predominant. In contrast, the dissociation of N_2 with an energy threshold of 24.3 eV [19] proves thermodynamically unfavorable within the corona discharge environment, with electron energies typically ranging between 1 and 10 eV. In addition, N_2 dissociation generates atomic nitrogen, which has a lower reactivity towards NO compared to O and OH radicals. Additionally, while CO_2 may dissociate, its products do not significantly participate in NO transformation pathways [20], thereby justifying its exclusion from consideration. Furthermore, the dissociation processes of CO, NO_x and C_xH_y species were deemed insignificant due to their comparatively low concentrations in the combustion gas, allowing for their omission from the kinetic analysis.

Ionic reactions were excluded from consideration, as the concentration of ions in the corona discharge is typically much lower than that of neutral species, their lifetimes are generally shorter, and ion-molecule reactions tend to be slower under these conditions compared to neutral radical reactions. Additionally, reactions involving low-concentration species were omitted, as their contribution to overall NO conversion would be statistically insignificant and their inclusion would unnecessarily complicate the model without enhancing its accuracy.

Similar simplified reaction sets, focusing on dominant pathways, have been successfully employed by other researchers including Jõgi et al. [8], who studied the NO oxidation in an N_2:O_2 mixture under the DBD discharge, and Mok et al. [12], who presented a model with experimental validation, demonstrating its adequacy in explaining observed NO conversion in the pulsed corona discharge. This simplification is supported by the empirical and mechanism research of Zhang et al. [21], who introduced the comprehensive study on NO_x removal in DBD. Their findings emphasized the negligible impact of high-threshold dissociation reactions, as well as reactions involving ions and other low-concentration species, on the overall process. The presented reaction pathway is, therefore, not only justified but necessary to simplify the reaction pathway while maintaining the accuracy of NO transformation modelling.

Several studies of NO conversion in DC corona discharge systems are presented. Wu et al. [22] investigated the NO conversion in a gas mixture of NO, N_2 and air by positive DC corona with different electrodes, and 82% NO conversion was observed. A similar

NO removal efficiency of 84.9% was obtained by Ji et al. [23] who applied a homemade DC corona reactor with positive polarity to a mixture with different fractions of SO_2, NO, N_2 and O_2. In contrast, Araji et al. [24] used a negative corona for $N_2/O_2/NO$ mixture, observing that the NO concentration reduced with corona energization and became zero at around 500 J/L. Wang et al. [25] simulated flue gas with a mixture of O_2, CO_2, H_2O, and NO using N_2 as the balance gas. NO removal by DC corona of both polarities was studied, and a 48% NO reduction was observed with much lower energy consumption for the positive discharge than for the negative one.

Nevertheless, a significant research gap remains in the NO removal from real small-scale combustion sources. To address this, the present work studies the NO transformation in the DC corona, building on previous work [14] that demonstrated the potential of DC corona ESPs for combined particulate matter and NO_x control in biomass combustion. The present study advances the field with several contributions: (i) a detailed analysis of the spatial distribution and reaction pathways of active species in both positive and negative corona offers new insights into the NO conversion mechanisms, highlighting the polarity impact on NO conversion; (ii) a predictive model, capable of accurately forecasting NO conversion efficiency under various operating conditions, was supported by experimental results.

This study applied an ESP with honeycomb-collecting electrodes to real combustion gases from a 5 kW automatic domestic wood pellet heater. The ESP operated under various positive and negative corona modes, with NO transformation predictions showing good agreement with experimental data. The energy effectiveness of the studied ESP was evaluated and compared with other existing technologies, and innovative design optimization strategies were proposed for both corona modes.

By bridging theoretical insights with practical implementation, this study provides a foundation for effective NO_x control solutions, improving residential air quality and supporting sustainable biomass energy use.

2. Materials and Methods

The emissions from low-power domestic heat source were controlled using the experimental setup in Figure 1.

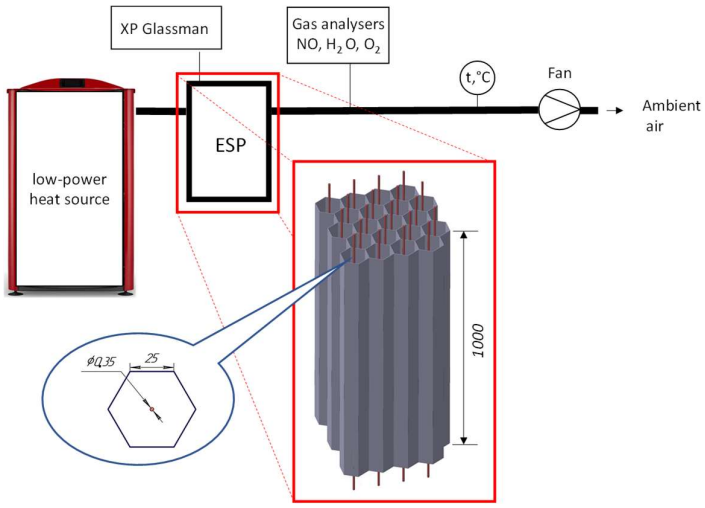


Figure 1. Experimental setup.

2.1. Setup

The NO conversion was studied using the experimental setup in Figure 1.

Combustion gases were generated in low-power heat source with a heat output of 5 kW, using wooden pellets as fuel. Combustion gases were consequently treated in an ESP and then expelled from the system with the help of a fan. The fan operated automatically to ensure a constant negative pressure of 15 Pa in the exhaust, based on the standard EN 303-5 [26]. The chemical composition of the wooden pellets can be found in [14]. The NO conversation was in special ESP. The collecting electrodes were honeycomb with a side length of 25 mm. Stainless-steel wires with a diameter of 0.25 mm were positioned along the axis of each hexagon cell to serve as discharge electrodes. The electrodes' active length was 1000 mm.

The ESP was supplied with high voltage from the XP Glassmann high-voltage power unit model PS/030R040-22. This power unit had a maximum output voltage of 30 kV and a maximum output current of 40 mA. The HV unit had a measurement accuracy for current better than 1%, and the voltage typical deviation was less than 2% of the rated output voltage, with recovery to within 0.1% in 1 ms.

To create different experimental conditions, the ESP was operated with both polarities, and each operation mode of the ESP was set to a specific stable current value, while the HV unit adjusted the voltage to maintain the selected current value. The high voltages ranged from the initial corona voltages to the maximal level limited by electrical breakdowns in the ESP or XP Glassman's technical capabilities.

2.2. Sampling and Evaluation

The Non-Dispersive Infra-Red (NDIR) detector by ABB was used to detect the composition of combustion gases, including NO concentration, with a measurement accuracy of 1.5% in the concentration range from 0 to 500 ppm. The NDIR analyzers were calibrated using appropriate calibration gases before each experimental series. The temperature of the combustion gases was measured using a thermocouple type K Class 1 with a measurement accuracy of ±1.5 °C over a range from −40 °C to +375 °C.

Sample results when the ESP operated in on/off regimes were used to evaluate the NO conversion efficiency. The concentration values were normalized to the volume unit of dry gas at 101.325 kPa, 0 °C, and reference O_2 at 10%.

The NO removal efficiency η_o was obtained as follows:

$$\eta_o = \left(1 - \frac{[NO]_{ESPon}}{[NO]_{ESPoff}}\right) \times 100\% \quad (1)$$

The specific input energy SIE [J/L], which presents the discharge electric power [W] transferred to a gas flow [L/s], was defined as follows

$$SIE = \frac{I \times U}{V} \quad (2)$$

where U is applied voltage [kV], I is electric current in ESP [mA] and V is the flow rate of combustion gas [L/s].

The modelling adequacy to practical measurements was estimated in this work using Pearson's chi-squared test [27]

$$\chi^2 = \sum \frac{(\eta_o - \eta_e)^2}{\eta_o} \quad (3)$$

with η_o and η_e representing, respectively, observed and predicted efficiency of NO conversion.

3. Results and Discussion

3.1. Parameters of Combustion Tests

Information on experimental conditions is presented in Table 2.

Table 2. Experimental conditions.

Parameter	Unit	Value
Combustion gas temperature	°C	125
Combustion gas flow rate *	L/s	9.8
Gas velocity in ESP	m/s	0.3
Content of/O_2/H_2O	vol %	13.0/7.8
The initial concentration of NO *	mg/m^3	130

* in dry flue gas (0 °C, 101.3 kPa); at reference O_2 = 10% vol.

The characteristics of the combustion gases were typical for small-scale domestic heating units [28], so the experimental conditions in this study are representative of typical small-scale biomass combustions. However, several unique aspects of this setup warrant discussion.

The initial NO concentration (130 mg/m^3) falls within the range typically observed in small-scale biomass combustion but is lower than concentrations used in some studies focusing on industrial applications (e.g., [29], who used up to 500 ppm NO). The flue gas in this study contained a relatively high water vapor content (8.31 vol%) compared to some previous works (e.g., [8] who used dry gas mixtures). This more adequately reflects combustion conditions and allows for a more accurate assessment of OH radical contributions to NO conversion.

The use of a honeycomb ESP differs from many previous studies that typically employed wire-plate or wire-cylinder configurations [22,25]. This geometry may enhance the uniformity of the electric field and potentially improve the overall efficiency of NO conversion.

The measured corona current and SIE, due to Formula (2), can be found in Figure 2 given by the applied voltage for both polarities. The minimal corona current of 0.1 mA corresponds to the voltage value of 5.0 kV/7.7 kV for negative/positive corona. The negative corona was stable but limited at 12 kV by XP Glassmann's current limit of 40 mA, whereas the corona of positive polarity was limited by sparks and breakdowns in the ESP at a voltage of 11.9 kV and current of 30 mA.

NO concentration remained unaffected until the ESP voltage was raised to 7.8 kV/8.4 kV for negative/positive corona. Further enhancements in voltage led to a notable reduction in NO concentrations observed from 130 mg/m^3 to 27/29 mg/m^3 for positive/negative polarity.

Energy consumption was higher for the negative corona in a whole range of varying voltages, even for values exceeding 10 kV when NO removal was higher for the positive corona. The SIE of 35 J/L ensured the 78-% NO reduction in ESP with the positive corona, while a similar removal was achieved in ESP at negative polarity with an SIE of 48 J/L. The energy consumption in studied ESP was similar to that reported in studies [22,25,30,31], which also employed a corona discharge.

The NO conversion observed in this study can be compared with other plasma-based NO_x abatement technologies, including advanced technologies such as NTP injection in the diesel exhaust system [32] and plasma-catalyst hybrid systems [33]. The studied ESP indicated potentially higher energy efficiency in comparison to the work of Jõgi et al. [8] who reported NO conversion efficiencies of up to 90% at an energy density of 100 J/L in a DBD reactor, or the results of Mok et al. [30], who achieved 90% NO removal at 120 J/L using a pulsed corona reactor.

Shadi et al. [33] used a hybrid system of DBD reactor and $LaMn_{0.9}Co_{0.1}O_3$ perovskite nanocatalyst for NO reduction in the NO_x/NH_3/air mixture; they demonstrated that a plasma–catalyst hybrid system achieved an enhanced removal efficiency exceeding 90% at

an energy input of 150 J/L, compared to 55% efficiency with plasma alone under the same energy conditions.

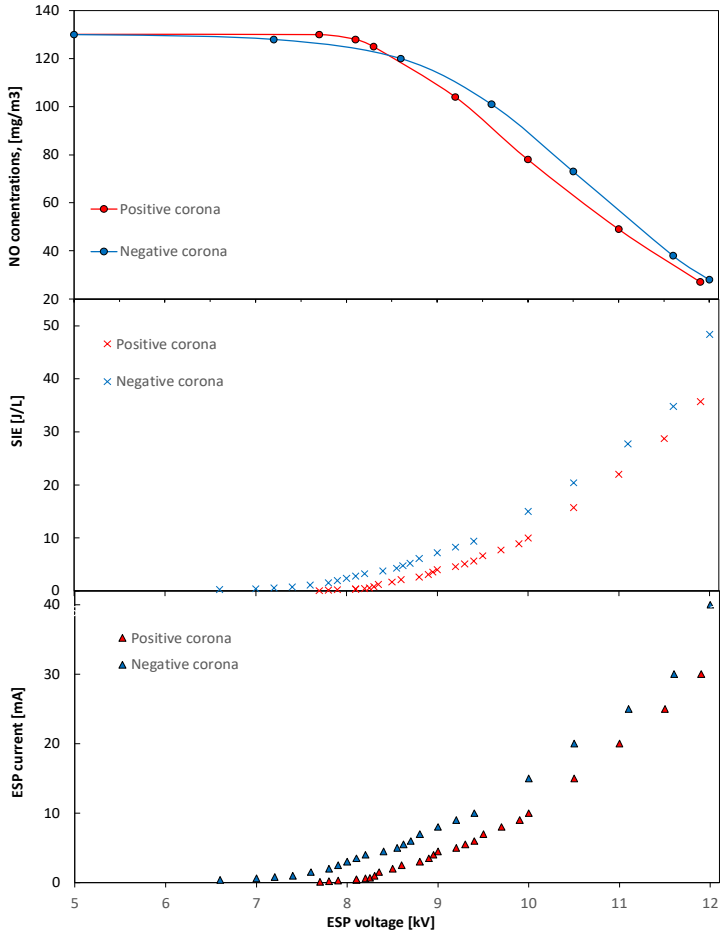


Figure 2. The corona current and SIE with the applied voltage.

Nguyen et al. [34] used a two-stage plasma–catalyst hybrid system with a honeycomb catalyst coated with Co, La, Pd, and Pt to a gas mixture of air, H_2O, NO and n-heptane. With 2.0% H_2O, 95% NO_x removal was reported at 56.5 J/L, whereas 89.0% of the NO was oxidized to NO_2.

In contrast, Kawakami et al. [35] used a discharge plasma reactor for simultaneous control of NO_x, PM, and HC in a diesel engine exhaust. While achieving a 70% NO_x removal efficiency, this method required a significantly higher SIE of approximately 600 J/L.

However, while less efficient, ESP technology can provide a more economically viable and less complex solution, which is particularly important for small-scale applications, where the complexity and cost of hybrid plasma–catalyst systems might be prohibitive. The advantage of ESP technology became more evident with the demonstrated potential of DC corona for combined PM and NO_x control.

Despite the relatively good performance of the studied ESP in NO abatement, it still falls short of some advanced hybrid plasma–catalyst systems. This suggests improvements, possibly through the development of more sophisticated electrode designs to optimize active species production. Significant improvements in energy efficiency can be achieved through a better understanding of the involved chemical mechanisms. Improvements in ESP technology can contribute to developing solutions for controlling emissions from small-scale combustions, where cost and simplicity are critical factors.

3.2. The Impact of ESP Energisation on Active Species Generation

In a DC corona discharge ESP, the electric field is highly non-uniform, varying significantly with the radial distance from the discharge electrode. This non-uniformity leads to varying rates of electron-induced dissociation at different points within the discharge region, resulting in spatially varying concentrations of active species. So, accurate prediction of NO transformation requires the electron densities and dissociation constants to be defined at each point of active species in the radial direction.

The local reduced electric field $\left(E_{(r)}/N\right)$, required to define dissociation constants, can be obtained for each point in the interelectrode gap, when the electric field distribution is known:

$$E_{(r)} = \sqrt{\frac{I}{2\pi l u_i \varepsilon_0} \cdot \left(1 - \left(\frac{r_0}{r}\right)^2\right) + \left(E_0 \cdot \frac{r_0}{r}\right)^2} \quad (4)$$

The electric field strength E_0 initiating corona discharge was determined by the Peek formula [36]

$$E_0 = A \times \beta + B\sqrt{\frac{\beta}{r_0}} \quad (5)$$

where A and B are constants evaluated experimentally. Originally derived for alternating voltages, this semiempirical formula yields results that align with negative DC corona when using the same values for A and B [37]. However, results differ when applied to DC corona with positive polarity, so other coefficients are required. The present research's values of A = 31.6/38.0 [kV/cm] and B = 8.47/8.06 [kV/cm$^{0.5}$] for a positive and a negative corona, respectively, were taken from [38], which studied corona generation between the electrodes of comparable dimensions and similar voltages.

The electron distribution can be solved from the coupled continuity equations for charge carriers (6)–(8) along with Poisson's Equation (9):

$$\frac{1}{r}\frac{d}{dr}\left(rq_e n_e \mu_e E_{(r)}\right) = (\alpha - \beta) q_e n_e \mu_e E_{(r)} \quad (6)$$

$$\frac{1}{r}\frac{d}{dr}\left(rq_e n_p \mu_p E_{(r)}\right) = -\alpha q_e n_e \mu_e E_{(r)} \quad (7)$$

$$\frac{1}{r}\frac{d}{dr}\left(rq_e n_n \mu_n E_{(r)}\right) = \beta q_e n_e \mu_e E_{(r)} \quad (8)$$

$$divE_{(r)} = -\frac{q_e\left(n_p - n_n - n_e\right)}{\varepsilon_0} \quad (9)$$

An ionization coefficient α can be defined as $\alpha = A_1 \exp(B_1/E)$ with $A_1 = 8.97 \times 10^3 \left[cm^{-1}\right]$ and $B_1 = 1.45 \times 10^5 [V/cm]$ [39]; attachment coefficient $\beta = 14.82 \times e^{(-34650/E)} \left[cm^{-1}\right]$ and the electron mobility $\mu_e = 1.2365 {E_{(r)}}^{-0.2165}$ were taken from [40].

Ion mobility is considered to be independent of the electric field. The present work employs the value for average positive ions' mobility u_i of 2.1 cm^2/(V × s), as stated by [41], confirmed by [42] and recently supported by [43]. The mobility for positive ions was here accepted to be 1.4 cm^2/(V × s), as stated by Adachi et al. [44], confirmed by [45] and supported by [46,47].

Figure 3 demonstrates the distribution of electrons and active species in the radial direction for negative A and positive B corona with a different ESP energization. Energization levels were selected to be maximally similar. The electron distribution was obtained by numerically solving Equations (6)–(9), considering the local electric field (Equation (3)). Densities for O and OH-radicals were obtained through R1–R2.

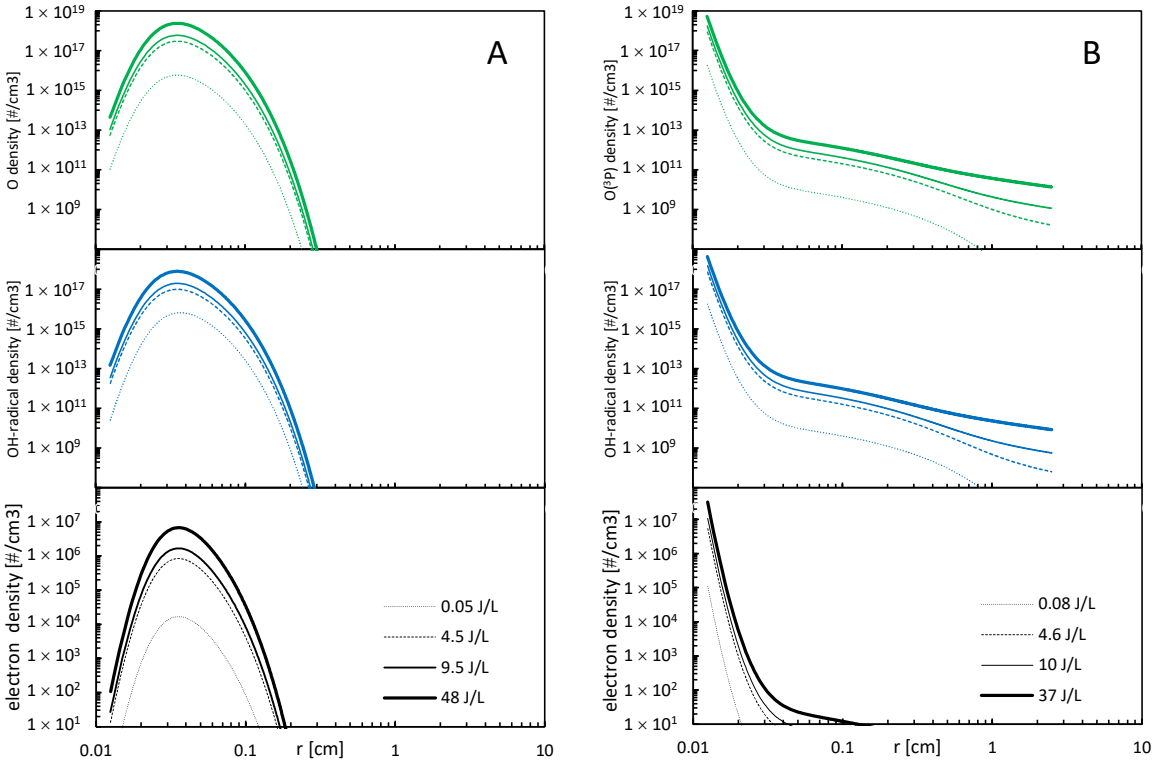


Figure 3. Electron and active species density distributions for negative (**A**) and positive (**B**) corona.

Chen and Davidson [48] comprehensively studied the distribution of the electric field in DC corona discharge under both positive and negative polarities. Their findings indicated that the local electric field distribution exhibited a sensitive increase with rising applied voltage, while the influence of discharge polarity was relatively minor. As a result, reaction rate constants for R1 and R2 turned out to be similar for both polarities.

The local electric field distribution was almost independent of discharge polarity, resulting in reaction constants turning out to be similar for both polarities. However, the electron distribution resulted in the ground-state oxygen atoms O and OH-radicals being more concentrated in the ionization region of a negative corona. This may lead to rapid NO conversion in this region but potentially leave a significant portion of the gas stream untreated. Contrarily, a more dispersed distribution of O and OH-radicals throughout the interelectrode gap in positive discharge suggests a more uniform reaction zone. This could result in more consistent NO conversion across the entire gas stream.

Based on principles of chemical kinetics, the lifetime of reactive species in combustion gases, such as atomic oxygen (O) and hydroxyl radicals (OH), can approximately be estimated as the ratio of their concentrations to the rate of reactions that deplete them.

Reactions R3, R6 and R8 are known to proceed with high rate constants (see Table 1). Oxygen atoms have an extremely short lifetime, well under a tenth of a microsecond, being rapidly consumed through multiple pathways, including ozone formation, direct NO oxidation, and back reactions with NO_2. This is consistent with those of [49], falling between 0.01 and 0.1 milliseconds. Similarly, forming HNO_2 and conversion to NO through reaction R9 limited the lifetime of OH-radicals well under 1 microsecond.

The interplay between spatial distribution and species lifetime creates distinct advantages and challenges for each corona type. In negative corona discharge, O and OH radicals are highly concentrated near the discharge electrode, creating an intense but localized reaction zone. This concentration pattern results in powerful conversion capabilities within a limited space but may lead to incomplete treatment of the gas stream. The challenge lies in ensuring that all gas molecules have sufficient exposure to these active regions.

Conversely, positive corona discharge exhibits a more dispersed distribution of active species throughout the interelectrode gap. This broader distribution enables more uniform treatment of the gas stream and potentially more efficient utilization of the active species. The wider reaction zone contributes to more consistent conversion rates and reduces the system's dependence on complex mixing requirements.

The ozone generation in Figure 4 was predicted through R3, considering destruction reaction R4, which was rather slow but more contributive for negative polarity. Both curves show signs of saturation at higher SIE levels, but this effect is more pronounced for negative corona. This could be due to increased ozone decomposition reactions and limitations in available oxygen for ozone formation.

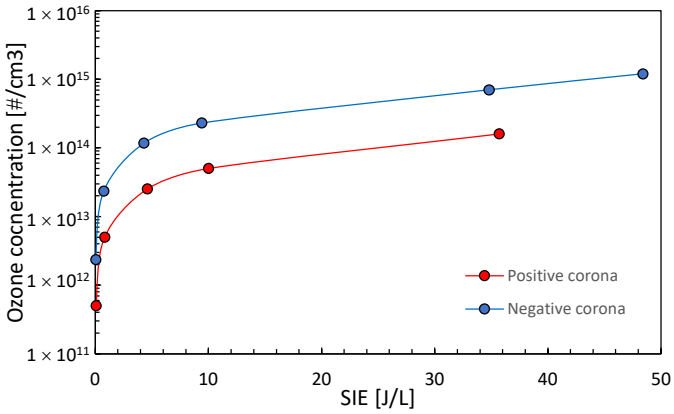


Figure 4. Ozone concentrations with SIE.

Negative corona consistently produces higher ozone concentrations across all SIE levels, with the difference becoming more pronounced at higher energization. The greater ozone yield for negative corona in the present research is in line with the previous conclusion stated in [50], supported in [51], and confirmed by experiments in [52,53].

The higher ozone concentrations in negative corona suggest a potentially greater contribution of ozone-mediated NO oxidation pathways compared to positive corona. However, the saturation effect in negative corona might limit the additional benefits of increasing SIE beyond certain levels.

3.3. The Impact of ESP Energization on NO Abatement

Under conditions of DC corona, the ionic wind generates turbulence in the combustion gases. For the studied ESP, the velocity of the ionic wind was defined to range, approximately, from about 0.01 to 1.5 m/s, depending on the ESP operation mode. Consequently, a period of about a tenth of a millisecond is reasonably assumed to be sufficient for combustion gas components to cross the distance from discharge to the collecting electrode. Additionally, diffusion initiated by concentration gradients contributes to the homogeneous distribution of species. Given this, ozone molecules with their longer lifetimes can be expected to be evenly distributed along the radial direction, while the distribution of ground-state oxygen atoms and OH radicals remains slightly affected by turbulence, tending to follow the pattern shown in Figure 3.

To analyze the importance of each active species in NO conversion, the theoretical changes in NO concentrations were calculated by solving a set of ordinary differential equations based on reactions R5-R10 along with reactions for ozone generation R3 and destruction R4.

NO oxidation by ground-state oxygen atoms (O) was accounted for through reaction R6 while considering the back reaction R8 to determine the NO concentration at the ESP

outlet. Similarly, changes in NO concentrations were considered due to a reduction by OH radicals, described by reaction R5 and factoring in the partial consumption of radicals as per reaction R9. This approach allowed for the calculation of NO conversion efficiency, based on Equation (1), for both oxidation and reduction scenarios. The initial concentrations of active species were derived from dissociation reactions R1 and R2, respectively, under various ESP energization levels.

The calculations were carried out for the above experiments' conditions and different ESP energization levels, and predicted efficiencies for NO oxidation by O and reduction by OH radicals are shown in Figure 5 as a function of SIE in ESP.

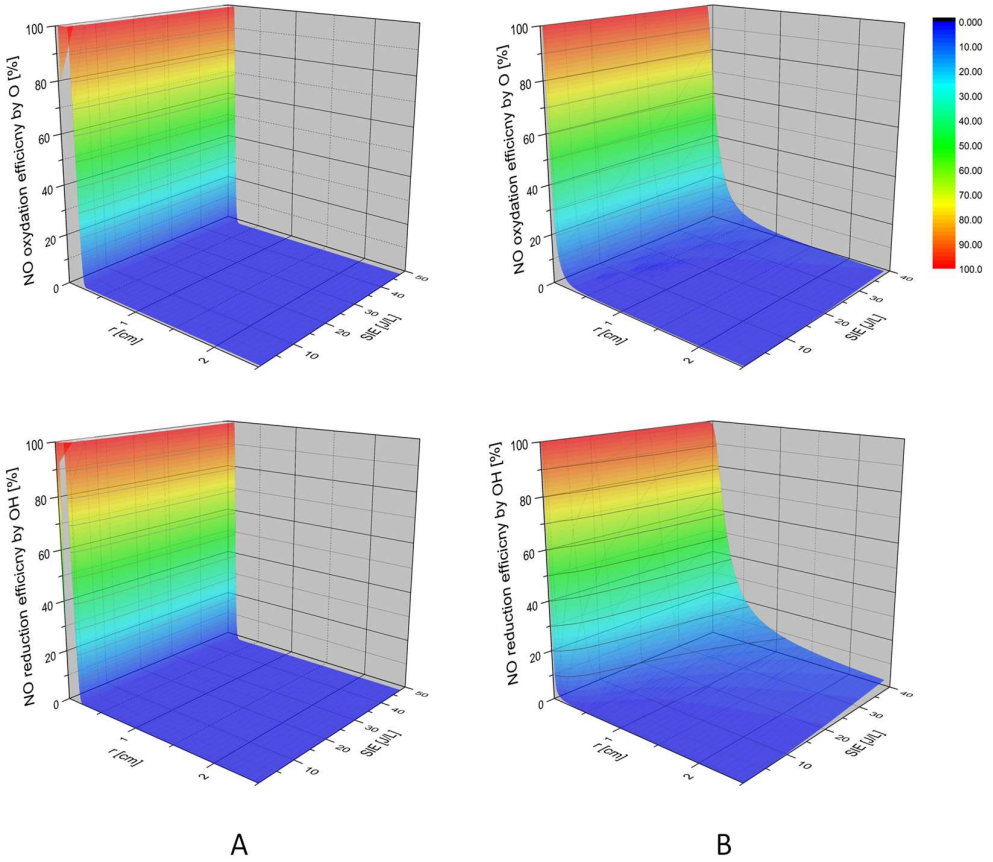


Figure 5. The efficiency of NO oxidation and reduction in negative (**A**) and positive (**B**) DC corona.

Neglecting the effect of diffusion and electrohydrodynamic turbulence, O and OH-radicals were suggested to be depleted once they were generated. For negative corona, these species were highly concentrated in the discharge electrode vicinity, ensuring the NO treatment efficiency was observed as high but limited only within the ionization zone with low dependence on the ESP energization. Conversely, the positive corona had a broader distribution of O and OH-radicals, making them more contributive in the whole interelectrode gap. The distribution of ozone in combustion gases was homogeneous, resulting in consistent oxidation of NO through R7 and being more contributive to negative corona.

The contribution of O, OH radical and ozone to NO transformation was obtained by integrating the above prediction results in the whole interelectrode gap. The results for each active species, along with the overall predicted efficiency for NO transformation, are compared with the measured results for both polarities (Figure 6).

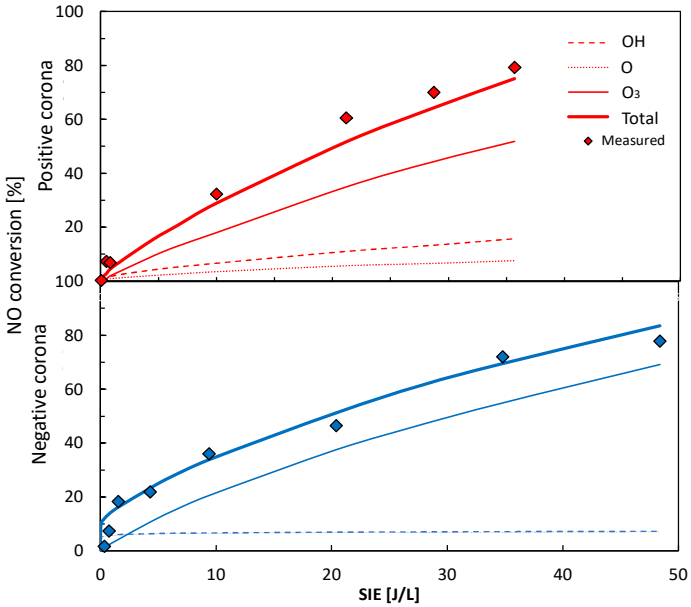


Figure 6. The efficiency of NO conversion with ESP energization.

For both polarities, the predicted NO conversion efficiency showed good general agreement with measured values across the range of SIE tested, validating the understanding of the primary reaction mechanisms of NO conversion.

For positive corona, the model successfully captured the overall trends, demonstrating the acceptable divergence to measured results: Pearson's criterion due to Formula (3) showed a deviation of 10% for low specific input energy (SIE) levels (<20 J/L) and 7% for higher energization regimes (SIE $\geq$ 20 J/L). The results' underestimation for positive corona might be due to underestimating the contribution of OH radicals in the dispersed reaction zone. A better overall agreement, within $\pm$5% of measured values, was observed for negative corona across the entire SIE range. The slight disagreements might result from oversimplifying the complex ozone-involved reactions or ignoring the effects of space charge.

To identify the most critical parameters affecting the NO conversion for each polarity, a simple sensitivity analysis was conducted by varying key gas parameters by $\pm$20% and observing the impact on NO conversion efficiency at 30 J/L. The results are presented in Table 3.

Table 3. The sensitivity of NO conversion in DC corona to gas parameters.

Gas Parameter	Sensitivity *	
	Positive Corona	Negative Corona
Temperature	$\pm$9%	$\pm$7%
Initial NO concentration	$\pm$13%	$\pm$11%
O_2 Concentration	$\pm$11%	$\pm$12%
H_2O concentration	$\pm$8%	$\pm$6%

* % change in NO conversion.

Positive corona generally shows higher sensitivity to parameter changes, suggesting it might be more responsive to optimization efforts but also potentially less stable under varying conditions. The effects of initial NO concentration and gas temperature are slightly higher in positive corona, possibly due to a more uniform reaction zone. Changing the O_2 concentration is slightly more critical for negative corona, likely due to its importance in

ozone generation. The ranging H_2O concentration, while less impactful overall, is more significant for positive corona, probably due to its role in OH radical formation.

3.4. The Polarity Effect on Energy Consumption

The SIE for NO conversion was different for positive and negative corona. One reason for this is that an ESP's current density is affected by ions' mobility and electron density, which are both different for negative and positive corona. As a result, the electric current in ESP, consisting of moved ions and electrons, differed for positive and negative voltage polarity at the same voltage. Also, ozone-involving reactions can contribute to the different energy consumption of NO_x removal.

When SIE was less than 10 J/L, NO was oxidized mostly by the ground-state oxygen atoms, with NO_2 as a major oxidation product. An increased energization of ESP resulted in the increased significance of the back-reaction R8. Jõgi et al. profoundly studied the importance of this back-reaction [8], noting the saturation of NO oxidation by O atoms, which makes the ozone reactions more significant. The enhanced ESP electrical parameters led to more intense ozone reactions, with the decomposition reaction R4 becoming more significant, thus shifting the equilibrium of reaction R3 to the left. The developed negative corona forced a further reverse reaction R10, supporting the saturation for NO oxidation [29], which was more intensive in negative corona under the same voltages for both polarities. More dispersed active species distribution may reduce the impact of back-reactions for positive corona.

The dominance of different reaction pathways in positive and negative corona provides valuable insights. The higher contribution of O and OH radical reactions for positive corona suggests a more direct and potentially more efficient NO conversion process, likely responsible for the higher energy efficiency observed in positive corona. The predominance of ozone-mediated oxidation, while effective, appears for negative corona to be more energy-intensive due to the energy required for ozone formation and potential ozone-consuming side reactions.

3.5. Optimization Strategies for Enhanced NO Conversion

The detailed analysis of reaction pathways and species distributions along with sensitivity analysis provides valuable insights for optimizing ESP design and operation, including improvement through electrode design optimization. Thus, for negative corona ESP, electrodes with multiple discharge points can be implemented to expand the high-intensity reaction zone; flow patterns can also be designed to maximize gas exposure to the region closest to the discharge electrode. For ESP with positive corona, the interelectrode gap can be optimized to take advantage of the more dispersed active species distribution.

Given the distinct advantages of each polarity, there may be potential for developing multi-stage ESP systems that alternate between positive and negative corona regions to combine the benefits of both discharges.

The sensitivity analysis reveals important considerations for system operation: the $\pm$9% change in NO conversion for a 20% temperature change in positive corona (compared to $\pm$7% in negative) suggests that positive corona systems may require more precise temperature control for optimal operation. The higher sensitivity to initial NO concentration in positive corona ($\pm$13% vs. $\pm$11%) indicates that positive corona systems might be more adaptable to varying NO levels but also potentially less stable under fluctuating conditions. The slightly higher sensitivity of negative corona to O_2 concentration ($\pm$12% vs. $\pm$11%) aligns with the observed importance of ozone-mediated reactions in negative corona. The slightly higher sensitivity of negative corona to O_2 concentration ($\pm$12% vs. $\pm$11%) aligns with the observed importance of ozone-mediated reactions in negative corona.

These considerations could significantly enhance the effectiveness of ESPs for NO_x control in small-scale biomass combustion systems.

4. Conclusions

NO conversion in DC corona discharge was experimentally and mechanistically studied under real biomass combustion conditions in a small-scale domestic heat source, offering findings more applicable to practical applications than studies using synthetic gas mixtures [22–25]. The main results are as follows:

1. Corona discharge polarity significantly impacts NO conversion and energy consumption: while a 78% NO reduction was achieved with ESP operation, positive corona required lower specific input energy (35 J/L) compared to negative corona (48 J/L). Despite achieving lower NO conversion than DBD reactors [8], plasma–catalyst hybrid systems [33,34] and pulsed corona [30], the DC corona ESP demonstrated lower energy consumption, making it a cost-effective option for small-scale applications.
2. The simplified reaction pathway, focusing on dominant reactions, demonstrates accuracy comparable to comprehensive reaction sets, such as those in [21], while being more practical for implementation.
3. The spatial distribution of active species differs between positive and negative corona, with negative corona O and OH radicals concentrated near the discharge electrode and producing 15–20% more ozone, with saturation effects observed above 30 J/L, while positive corona created a more dispersed distribution of active species. Reactions with O and OH radicals dominate at low SIE, while ozone-mediated reactions prevail above 10 J/L for both polarities.
4. At 30 J/L, sensitivity analysis showed that ±20% fluctuations in temperature, initial NO concentration, oxygen, and water vapor affected NO conversion efficiency for positive corona by ±9%, ±13%, ±11%, and ±8%, respectively, while negative corona showed corresponding variations of ±7%, ±11%, ±12%, and ±6%.
5. The ESP technology for small-scale biomass heating systems may be potentially improved through dual-polarity systems, optimized electrode designs, and improvements to adjust flow patterns.

Further investigation into the implementation of the results of the present study along with research on long-term stability and maintenance of improved ESPs would enhance the applicability of these findings to small-scale combustion scenarios.

Author Contributions: Conceptualization, O.M.; methodology, O.M.; software, K.K.; validation, J.H, L.K. and F.H.; formal analysis, O.M.; investigation, O.M.; resources, J.R.; data curation, M.B.; writing—original draft preparation, O.M.; writing—review and editing, O.M.; visualization, L.K.; supervision, J.H.; project administration, J.R.; funding acquisition, J.R. All authors have read and agreed to the published version of the manuscript.

Funding: This work was supported by the project LIFE-IP SK AQ Improvement "Enhancing the implementation of Air Quality Management Plans in Slovakia by strengthening capacities and competencies of regional and local authorities and promoting air quality measures", identification number LIFE18 IPE/SK/000010. The project has received funding from the LIFE Programme of the European Union and is co-financed by the state budget of the Czech Republic through the Ministry of Environment. The European Union also financially supported this work under the REFRESH—Research Excellence For Region Sustainability and High-tech Industries project No. CZ.10.03.01/00/22_003/0000048 via the Operational Programme Just Transition.

Institutional Review Board Statement: Not applicable.

Informed Consent Statement: Not applicable.

Data Availability Statement: The data used in this research are available in the public domain.

Conflicts of Interest: The authors declare no conflicts of interest.

References

1. Eurostat. Available online: http://ec.europa.eu/eurostat/data/database (accessed on 5 June 2024).
2. Wang, L.; Xuan, C.; Zhang, X.; Sun, R.; Cheng, X.; Wang, Z.; Ma, C. NO_x Adsorption Mechanism of Coal-Based Activated Carbon Modified with Trace Potassium: In Situ DRIFTS and DFT Study. *Energy Fuels* **2022**, *36*, 7633–7650. [CrossRef]
3. Gómez-García, M.A.; Pitchon, V.; Kiennemann, A. Pollution by nitrogen oxides: An approach to NOx abatement by using sorbing catalytic materials. *Environ. Int.* **2005**, *31*, 445–467. [CrossRef]
4. Liu, J.; Liu, J.; Zhang, G. Recent Advances in NO Reduction with NH_3 and CO over Cu-Ce Bimetallic and Derived Catalysts. *Catalysts* **2024**, *14*, 819. [CrossRef]
5. Zi, X.; Ye, J.; Cheng, Y.; Li, S.; Li, X.; Li, X.; Qiu, W.; Song, L. The Effect of CeO_2 on the Catalytic Activity and SO_2 Resistance of the V_2O_5-MoO_3/TiO_2 Catalyst Prepared Using the Ball Milling Method for the NH_3-SCR of NO. *Catalysts* **2024**, *14*, 794. [CrossRef]
6. Guo, Q.; Zhao, M.; Fan, H.; Zhu, R.; Zhong, R.; Bai, X. Low-Temperature NH3-SCR Technology for Industrial Application of Waste Incineration: An Overview of Research Progress. *Catalysts* **2024**, *14*, 766. [CrossRef]
7. Ciupek, B.; Urbaniak, R.; Kinalska, D.; Nadolny, Z. Flue Gas Recirculation System for Biomass Heating Boilers—Research and Technical Applications for Reductions in Nitrogen Oxides (NO_x) Emissions. *Energies* **2024**, *17*, 259. [CrossRef]
8. Jõgi, I.; Levoll, E.; Raud, J. Plasma oxidation of NO in O_2:N_2 mixtures: The importance of back-reaction. *Chem. Eng. J.* **2016**, *301*, 149–157. [CrossRef]
9. Wang, J.; Yi, H.; Tang, X.; Zhao, S.; Gao, F. Simultaneous removal of SO_2 and NOx by catalytic adsorption using γ-Al_2O_3 under the irradiation of non-thermal plasma: Competitiveness, kinetic, and equilibrium. *Chem. Eng. J.* **2020**, *384*, 123334. [CrossRef]
10. Masuda, S.; Nakao, H. Control of NO_x by positive and negative pulsed corona discharges. *IEEE Trans. Ind. Appl.* **1990**, *26*, 374–383. [CrossRef]
11. Hu, X.; Zhang, J.-J.; Mukhnahallipatna, S.; Hamann, J.; Biggs, M.J.; Agarwal, P. Transformations and destruction of nitrogen oxides—NO, NO_2 and N_2O—In a pulsed corona discharge reactor. *Fuel* **2003**, *82*, 1675–1684. [CrossRef]
12. Mok, Y.S.; Kim, J.H.; Nam, I.-S.; Ham, S.W. Removal of NO and Formation of Byproducts in a Positive-Pulsed Corona Discharge Reactor. *Ind. Eng. Chem. Res.* **2000**, *39*, 3938–3944. [CrossRef]
13. Kossyi, I.A.; Kostinsky, A.Y.; Matveyev, A.A.; Silakov, V.P. Kinetic scheme of the non-equilibrium discharge in nitrogen-oxygen mixtures. *Plasma Sources Sci. Technol.* **1992**, *1*, 207. [CrossRef]
14. Molchanov, O.; Krpec, K.; Horák, J.; Kubonová, L.; Hopan, F.; Ryšavý, J. Combined control of PM and NO_x emissions by corona discharge. *Sep. Purif. Technol.* **2024**, *345*, 127359. [CrossRef]
15. Manion, J.A.; Huie, R.E.; Levin, R.D.; Burgess, D.R., Jr.; Orkin, V.L.; Tsang, W.; McGivern, W.S.; Hudgens, J.W.; Knyazev, V.D.; Atkinson, D.B. NIST Chemical Kinetics Database, NIST Standard Reference Database 17, Version 7.0 (Web Version), Release 1.6.8, Data version 2015.09, National Institute of Standards and Technology, Gaithersburg, MD, USA. Available online: https://kinetics.nist.gov/ (accessed on 3 September 2024).
16. Atkinson, R.; Baulch, D.L.; Cox, R.A.; Crowley, J.N.; Hampson, R.F.; Hynes, R.G.; Jenkin, M.E.; Rossi, M.J.; Troe, J. Evaluated kinetic and photochemical data for atmospheric chemistry: Volume I—Gas phase reactions of O_x, HO_x, NO_x and SO_x species. *Atmos. Chem. Phys.* **2004**, *4*, 1461–1738. [CrossRef]
17. Itikawa, Y.; Mason, N. Cross Sections for Electron Collisions with Water Molecules. *J. Phys. Chem. Ref. Data* **2005**, *34*, 1–22. [CrossRef]
18. Cosby, P.C. Electron-impact dissociation of oxygen. *J. Chem. Phys.* **1993**, *98*, 9560–9569. [CrossRef]
19. Hagstrum, H.D. Ionization by Electron Impact in CO, N_2, NO, and O_2. *Rev. Mod. Phys.* **1951**, *23*, 185–203. [CrossRef]
20. Raizer, Y.P.; Allen, J.E. *Gas Discharge Physics*; Springer: Berlin/Heidelberg, Germany, 1991; Volume 1.
21. Zhang, W.; Wang, Z.; Guo, Y.; Yang, M.; Li, Z.; Zhang, J.; Chang, C.; Ji, Y. Experimental and mechanism research on the NO_x removal by a novel liquid electrode dielectric barrier discharge reactor. *Chem. Eng. J.* **2022**, *443*, 136375. [CrossRef]
22. Wu, Z.L.; Gao, X.; Luo, Z.Y.; Wei, E.Z.; Zhang, Y.S.; Zhang, J.Z.; Ni, M.J.; Cen, K.F. NO_x Treatment by DC Corona Radical Shower with Different Geometric Nozzle Electrodes. *Energy Fuels* **2005**, *19*, 2279–2286. [CrossRef]
23. Ji, W.; Yang, C.; Qu, G.; Zhou, J.; Chen, Y.; Tang, H.; Li, Z.; Xie, R.; Ning, P. Purification mechanism of corona discharge coupled with dimethyl sulfoxide microemulsion for simultaneous desulfurization and denitrification. *Sep. Purif. Technol.* **2022**, *300*, 121866. [CrossRef]
24. Arai, M.; Saito, M.; Yoshinaga, S. Effect of oxygen on NO_x removal in corona discharge field: NOx behavior without a reducing agent. *Combust. Sci. Technol.* **2004**, *176*, 1653–1665. [CrossRef]
25. Wang, M.; Zhu, T.; Wang, H. Oxidation and Removal of NO From Flue Gas by DC Corona Discharge Combined With Alkaline Absorption. *IEEE Trans. Plasma Sci.* **2011**, *39*, 704–710. [CrossRef]
26. Érces, N.; Kajtár, L. Heating boilers—Part 5: Heating boilers for solid fuels, manually and automatically stoked, nominal heat output of up to 500 kW—Terminology, requirements, testing and marking. *Energies* **2021**, *14*, 2926.

27. Pearson, K.X. On the criterion that a given system of deviations from the probable in the case of a correlated system of variables is such that it can be reasonably supposed to have arisen from random sampling. *Lond. Edinb. Dublin Philos. Mag. J. Sci.* **1900**, *50*, 157–175. [CrossRef]
28. Jaworek, A.; Sobczyk, A.T.; Marchewicz, A.; Krupa, A.; Czech, T. Particulate matter emission control from small residential boilers after biomass combustion. A review. *Renew. Sustain. Energy Rev.* **2021**, *137*, 110446. [CrossRef]
29. Zhang, Z.; Xi, H.; Zhou, S.; Zhou, W.; Shreka, M. Efficient removal of NO_x from simulated marine exhaust by using O_3-Na_2SO_3: Experimental factors and optimization analysis. *Fuel* **2022**, *313*, 122659. [CrossRef]
30. Mok, Y.S.; Nam, I.-S. Modeling of pulsed corona discharge process for the removal of nitric oxide and sulfur dioxide. *Chem. Eng. J.* **2002**, *85*, 87–97. [CrossRef]
31. Wang, M.; Sun, Y.; Zhu, T. Removal of NO_x, SO_2, and Hg From Simulated Flue Gas by Plasma—Absorption Hybrid System. *IEEE Trans. Plasma Sci.* **2013**, *41*, 312–318. [CrossRef]
32. Chen, X.; Shi, Y.; Cai, Y.; Xie, J.; Yang, Y.; Hou, D.; Fan, Y. Effect of non-thermal plasma injection flow rate on diesel particulate filter regeneration at room temperature. *Carbon Lett.* **2024**, *34*, 1075–1089. [CrossRef]
33. Shadi, Z.; Rahemi, N.; Allahyari, S.; Tasbihi, M. Low-temperature reduction of NO_x with NH_3 using a hybrid system of non-thermal plasma-$LaMn_{0.9}CO_{0.1}O_3$ perovskite nanocatalyst. *J. Environ. Chem. Eng.* **2024**, *12*, 114973. [CrossRef]
34. Nguyen, D.B.; Matyakubov, N.; Saud, S.; Heo, I.; Kim, S.-J.; Kim, Y.J.; Lee, J.H.; Mok, Y.S. High-Throughput NOx Removal by Two-Stage Plasma Honeycomb Monolith Catalyst. *Environ. Sci. Technol.* **2021**, *55*, 6386–6396. [CrossRef]
35. Kawakami, K.; Watatani, K.; Yamasaki, H.; Kuroki, T.; Okubo, M. Performance evaluation of PM, NO_x, and hydrocarbon removal in diesel engine exhaust by surface discharge-induced plasma. *J. Hazard. Mater.* **2024**, *462*, 132685. [CrossRef] [PubMed]
36. Peek, F.W. The Law of Corona and the Dielectric Strength of Air-II. *Trans. Am. Inst. Electr. Eng.* **1912**, *XXXI*, 1051–1092. [CrossRef]
37. Whitehead, J.B.; Brown, W.S. The Electric Strength of Air.-VII. *Trans. Am. Inst. Electr. Eng.* **1917**, *XXXVI*, 169–205. [CrossRef]
38. Farwell, S.P. The Corona Produced by Continuous Potentials. *Trans. Am. Inst. Electr. Eng.* **1914**, *XXXIII*, 1631–1671. [CrossRef]
39. Eliasson, B.; Kogelshatz, U. Basic data for modeling of electrical discharges in gases: Oxygen report. *Tech. Rep.* 1986. Available online: https://books.google.cz/books?id=5FJCAQAAIAAJ (accessed on 6 July 2024).
40. Chen, J.; Davidson, J.H. Electron Density and Energy Distributions in the Positive DC Corona: Interpretation for Corona-Enhanced Chemical Reactions. *Plasma Chem. Plasma Process.* **2002**, *22*, 199–224. [CrossRef]
41. Robinson, M. Electrostatic Precipitation in Air Pollution Control, Part I (W. Strauss, ed.). Wiley-Interscience: New York, NY, USA, 1971; pp. 256–281.
42. Strauss, W. *Industrial Gas Cleaning*; Pergamon Press: Oxford, UK, 1975.
43. Ning, Z.; Podlinski, J.; Shen, X.; Li, S.; Wang, S.; Han, P.; Yan, K. Electrode geometry optimization in wire-plate electrostatic precipitator and its impact on collection efficiency. *J. Electrost.* **2016**, *80*, 76–84. [CrossRef]
44. Adachi, M.; Kousaka, Y.; Okuyama, K. Unipolar and bipolar diffusion charging of ultrafine aerosol particles. *J. Aerosol Sci.* **1985**, *16*, 109–123. [CrossRef]
45. Reischl, G.P.; Mäkelä, J.M.; Karch, R.; Necid, J. Bipolar charging of ultrafine particles in the size range below 10 nm. *J. Aerosol Sci.* **1996**, *27*, 931–949. [CrossRef]
46. Marquard, A.; Meyer, J.; Kasper, G. Unipolar Field and Diffusion Charging in the Transition Regime—Part II: Charging Experiments. *Aerosol Sci. Technol.* **2007**, *41*, 611–623. [CrossRef]
47. Bürger, P.; Riebel, U. Electrostatic charging and precipitation of nanoparticles in technical nitrogen: Highly efficient diffusion charging by hot free electrons. *J. Aerosol Sci.* **2020**, *141*, 105495. [CrossRef]
48. Chen, J.; Davidson, J.H. Model of the Negative DC Corona Plasma: Comparison to the Positive DC Corona Plasma. *Plasma Chem. Plasma Process.* **2003**, *23*, 83–102. [CrossRef]
49. Wang, P.; Chen, J. Numerical modelling of ozone production in a wire–cylinder corona discharge and comparison with a wire–plate corona discharge. *J. Phys. D Appl. Phys.* **2009**, *42*, 035202. [CrossRef]
50. Viner, A.S.; Lawless, P.A.; Ensor, D.S.; Sparks, L.E. Ozone generation in DC-energized electrostatic precipitators. *IEEE Trans. Ind. Appl.* **1992**, *28*, 504–512. [CrossRef]
51. Chen, J.; Davidson, J.H. Ozone Production in the Negative DC Corona: The Dependence of Discharge Polarity. *Plasma Chem. Plasma Process.* **2003**, *23*, 501–518. [CrossRef]
52. Chen, J.; Davidson, J.H. Ozone Production in the Positive DC Corona Discharge: Model and Comparison to Experiments. *Plasma Chem. Plasma Process.* **2002**, *22*, 495–522. [CrossRef]
53. Junhong, C.; Pengxiang, W. Effect of relative humidity on electron distribution and ozone production by DC coronas in air. *IEEE Trans. Plasma Sci.* **2005**, *33*, 808–812. [CrossRef]

Disclaimer/Publisher's Note: The statements, opinions and data contained in all publications are solely those of the individual author(s) and contributor(s) and not of MDPI and/or the editor(s). MDPI and/or the editor(s) disclaim responsibility for any injury to people or property resulting from any ideas, methods, instructions or products referred to in the content.